

Underwater Image Enhancement: Using Wavelength Compensation and Image Dehazing (WCID)

John Y. Chiang¹, Ying-Ching Chen¹, and Yung-Fu Chen²

¹ Department of Computer Science Engineering,
National Sun Yat-sen University, Kaohsiung, Taiwan
chiang@cse.nsysu.edu.tw,
m983040018@student.nsysu.edu.tw

² Department of Management Information Systems and
Institute of Biomedical Engineering and Material Science,
Central Taiwan University of Science and Technology, Taichung, Taiwan
yfchen@ctust.edu.tw

Abstract. Underwater environments often cause color scatter and color cast during photography. Color scatter is caused by haze effects occurring when light reflected from objects is absorbed or scattered multiple times by particles in the water. This in turn lowers the visibility and contrast of the image. Color cast is caused by the varying attenuation of light in different wavelengths, rendering underwater environments bluish. To address distortion from color scatter and color cast, this study proposes an algorithm to restore underwater images that combines a dehazing algorithm with wavelength compensation (WCID). Once the distance between the objects and the camera was estimated using dark channel prior, the haze effects from color scatter were removed by the dehazing algorithm. Next, estimation of the photography scene depth from the residual energy ratios of each wavelength in the background light of the image was performed. According to the amount of attenuation of each wavelength, reverse compensation was conducted to restore the distortion from color cast. An underwater video downloaded from the Youtube website was processed using WCID, Histogram equalization, and a traditional dehazing algorithm. Comparison of the results revealed that WCID simultaneously resolved the issues of color scatter and color cast as well as enhanced image contrast and calibrated color cast, producing high quality underwater images and videos.

Keywords: Underwater image, Image dehazing, Wavelength compensation.

1 Introduction

Capturing clear images in underwater environments is an important issue of ocean engineering [1]. The effectiveness of applications such as underwater navigational monitoring and environment evaluation depend on the quality of underwater images. Capturing clear images underwater is challenging, mostly due to haze caused by color scatter in addition to color cast from varying light attenuation in different wavelengths [2]. Color scatter and color cast result in blurred subjects and lowered contrast in

underwater images. In Figure 1, for example, the yellow coral reef at the bottom of the image and the yellow fish in the upper-right corner are indistinct because of color cast; the school of Carangidae, the diver, and the reef in the back are unclear due to scattering.



Fig. 1. Blurry and Bluish Effects from Haze and Color cast in Underwater Images

Haze is caused by suspended particles such as sand, minerals, and plankton that exist in lakes, oceans, and rivers. As light reflected from objects proceeds towards the camera, a portion of the light meets these suspended particles, which absorbs and scatters the light (Fig. 2). In environments without blackbody emission [3], scattering often expands to multiple scattering, further dispersing the beam into homogeneous background light.

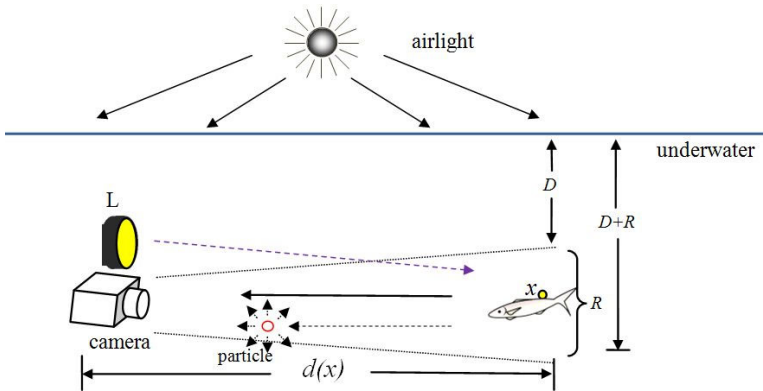


Fig. 2. Natural Light Illuminates an Underwater Scene Point x and the Reflected Light Travels to the Camera by Direct Transmission and Scattering

The underwater image of light after scattering can be expressed as the weighted sum of directly transmitted reflected light and scattered background light [4]:

$$I_{\lambda}(x) = J_{\lambda}(x)t_{\lambda}(x) + B_{\lambda}(1 - t_{\lambda}(x)), \lambda \in \{R, G, B\}, \tag{1}$$

$$t_{\lambda}(x) = \frac{E_o(\lambda, d(x))}{E_I(\lambda, 0)} = 10^{-\beta(\lambda)d(x)} = (Rer(\lambda))^{d(x)}, \tag{2}$$

where x is a point in the image; λ is the wavelength of the light; $I_i(x)$ is the image captured by the camera; $J_i(x)$ is the reflected light that is directly transmitted. Light attenuates when passing through a medium [5]; the residual energy ratio (Rer) indicates the ratio of residual energy to initial energy for every unit of distance. Supposing the energy of a light beam before and after it passes through a medium with a length of $d(x)$ is $E_i(\lambda, 0)$ and $E_o(\lambda, d(x))$, respectively; $t_\lambda(x)$ represents the residual energy ratio of the light beam after passing through the medium. Due to the fact that $t_\lambda(x)$ depends on wavelength λ and $d(x)$, the distance between x and the camera, $t_\lambda(x)$, causes color scatter and color cast.

The Rer of various light wavelengths differ in water [6]. As illustrated in Figure 3, red light possesses longer wavelength and lower frequency, thereby attenuating faster than blue light. This results in the blueness of most underwater images.

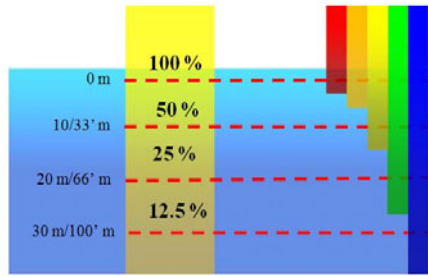


Fig. 3. Penetration of Light of Various Wavelengths through Water; Blue Light is the Strongest and Red Light is the Weakest

In addition to wavelength, the residual energy ratio $t_\lambda(x)$ is also influenced by the salt ratio in the water [7]. Using the amount of suspended particles and salt ratio, ocean water falls into three categories: general ocean water (Ocean Type 1), turbid tropical-subtropical water (Ocean Type 2), and mid-latitude water (Ocean Type 3) [7]. For every meter of general ocean water that a light beam passes through, the Rer values of red light ($700\mu m$), green light ($520\mu m$), and blue light ($440\mu m$) are 82 %, 95 %, and 97.5 %. The Rer in various environments can be adjusted with general ocean water as the standard. Suppose an incident light beam A from the air forms background light B at depth D after attenuation and multiple scattering; background light is in correspondence with the brightest portion of the image. The relationship between incident light beam A and background light B can be expressed with an energy attenuation model:

$$E_B(\lambda, D) = E_A(\lambda, 0) \times (Rer(\lambda))^D, \lambda \in \{R, G, B\}, \tag{3}$$

where $E_A(\lambda, 0)$ and $E_B(\lambda, D)$ are the energy of the incident light and the background light with wavelength λ . The Rer values of various wavelengths are [6]:

$$Rer(\lambda) = \begin{cases} 0.8\sim 0.85 & \text{if } \lambda = 650 \sim 750\mu m, \\ 0.93\sim 0.97 & \text{if } \lambda = 490 \sim 550\mu m, \\ 0.95\sim 0.99 & \text{if } \lambda = 400 \sim 490\mu m. \end{cases} \tag{4}$$

Conventionally, the processing of underwater images is directed either towards calibrating distortion from color scatter or from color cast. Research on improving the former has included applying the properties of polarizers to enhance image contrast and visibility [8], using image dehazing to eliminate hazing effects and enhance image contrast [9], and combining point spread functions (PSF) and modulation transfer function (MTF) in coordination with wavelet decomposition to enhance the high frequency areas in images [10] and increase visibility. Although the approaches above can augment contrast and sharpen images, they cannot solve the issue of color cast. Research regarding improvement of color cast includes using the properties of light transmitting through water to provide energy compensation using the attenuation differences between various wavelengths [11] and employing histogram equalization on underwater images to balance the luminance distributions of color [12]. Despite the improvement in the color distortion of objects, these methods cannot repair the image blurriness caused by color scatter.

The WCID algorithm proposed in this study combines a dehazing algorithm and energy compensation. Dark channel prior is used to estimate the distance of the object to the camera, and the dehazing algorithm removes the hazing effects caused by color scatter. Once underwater background light and the R_{er} values of various wavelengths of light are used to estimate the depth of the underwater scene, reverse compensation according to each wavelength is carried out to restore the color cast from water depth. With WCID, expensive optical instruments or distance estimation by two images is no longer required; WCID can effectively enhance visibility in underwater images and restore the original colors, obtaining high quality visual effects.

2 Underwater Image Model

The actual environment of underwater photography is as seen in Figure 2. Natural light from above the water attenuates while traveling to underwater depth D to illuminate the underwater scene. At x , a point within the scene, the reflected light travels a distance of $d(x)$ to the camera to form the image. Color scatter is a result of light absorption and multiple scattering by suspended particles on the way to the camera; color cast is due to the inconsistent attenuation of light at different wavelengths and occurs in both the depth D and the distance $d(x)$. Within the depth range R from the top of the image (D) to the bottom ($D+R$), the degree of attenuation varies in each area of the image, thereby necessitating estimation of underwater depth at each point for compensation. In general, to overcome insufficient lighting in an underwater photographic environment, an artificial light source such as L is used to assist photography. While compensating the energy lost in attenuation within the depth range, the luminance contributed by L must be considered to avoid overcompensation. The WCID algorithm follows an underwater image model for reverse compensation by first removing color scatter and color cast from distance $d(x)$ and then restoring the color cast from depth D . The amount of energy attenuated within the image range R and the luminance of the artificial light source L are then considered before carrying out appropriate compensation. The following section discusses the estimation of $d(x)$, depth D , artificial light source L , and depth range R as well as the procedure for energy compensation.

2.1 Distance between the Camera and the Object: $d(x)$

Conventional estimation of the distance between an object in an image and the camera requires two images for parallax. In a hazy environment, haze increases with distance; consequently, evaluating the concentration of haze in a single image is sufficient to predict the distance $d(x)$ between the object in the scene and the camera [4]. Using dark channel prior, $d(x)$ can be derived [14]. Dark channel refers to the phenomenon of there being at least one pixel with a near zero brightness value in the area $\Omega(x)$ surrounding any given point x in an outdoor haze-free image. Therefore the dark channel J_{dark} of an outdoor haze-free image can be defined as:

$$J_{dark}(x) = \min_{\lambda} \left(\min_{y \in \Omega(x)} (J_{\lambda}(y)) \right) \approx 0, \lambda \in \{R, G, B\}. \quad (5)$$

Taking the min operation in the local patch $\Omega(x)$ on the hazy image $I_{\lambda}(x)$ in Eq. (1), we have

$$\min_{y \in \Omega(x)} (I_{\lambda}(y)) = \min_{y \in \Omega(x)} \{J_{\lambda}(y)t_{\lambda}(y) + B_{\lambda}(1-t_{\lambda}(y))\}, \lambda \in \{R, G, B\}, \quad (6)$$

since B_{λ} is the homogeneous background light and the residual energy ratio $t_{\lambda}(y)$ in a local patch $\Omega(x)$ is essentially a constant [13], Eq. (6) can be further simplified as:

$$\min_{y \in \Omega(x)} (I_{\lambda}(y)) \approx \min_{y \in \Omega(x)} (J_{\lambda}(y))t_{\lambda}(x) + B_{\lambda}(1-t_{\lambda}(x)), \lambda \in \{R, G, B\}. \quad (7)$$

Rearrange the above equation and perform one more min operation among all three color channels:

$$\min_{\lambda \in \{R, G, B\}} \left\{ \frac{\min_{y \in \Omega(x)} (I_{\lambda}(y))}{B_{\lambda}} \right\} \approx \min_{\lambda \in \{R, G, B\}} \left\{ \frac{\min_{y \in \Omega(x)} (J_{\lambda}(y))}{B_{\lambda}} \cdot t_{\lambda}(x) \right\} + \min_{\lambda \in \{R, G, B\}} (1-t_{\lambda}(x)), \quad (8)$$

since J_{dark} is very close to 0 as shown in Eq. (5), the first term on the right-hand side of Eq. (8) can be regarded as 0. After this simplification, Eq. (8) can be rewritten as:

$$\tilde{t}(x) = \min_{\lambda \in \{R, G, B\}} t_{\lambda}(x) \approx 1 - \min_{\lambda \in \{R, G, B\}} \left\{ \frac{\min_{y \in \Omega(x)} (I_{\lambda}(y))}{B_{\lambda}} \right\}, \quad (9)$$

where $\tilde{t}(x)$ changes with $d(x)$, the distance between a point x on an object and the camera. The depth map of Fig. 1 is shown in Fig. 4(a).

The calculation of dark channel prior is based on blocks, creating a less accurate depth map. By applying image matting to repartition the depth map of Figure 4, the distortion of mosaics can be improved [14] for better capture of object contours.

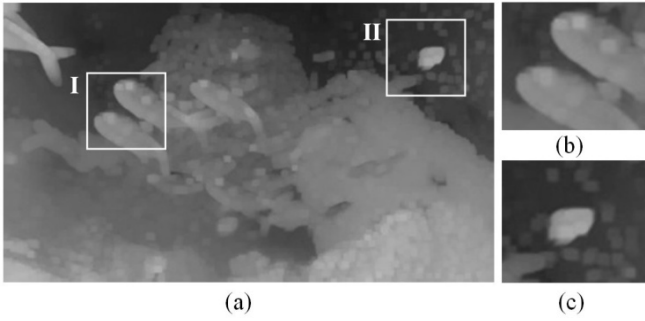


Fig. 4. (a) Depth Map from Estimating Distance between the Object and the Camera Using Dark Channel Prior; (b) Blow Up of Frame I; (c) Blow Up of Frame II

Image matting requires input of a preliminary partitioned depth map (Fig. 4) and the original image. Objects are detected using the relationship between the mean color value and the covariance of a local area w_x within the image and then the preliminary partitioned depth map is corrected using the relationship among the objects themselves. Taking the depth map of Figure 4(a) as t_{coarse} and the improved depth map as t_{refine} , t_{coarse} and t_{refine} can be expressed as:

$$(\mathbf{L} + \Lambda \mathbf{U}) \mathbf{t}_{\text{refined}} = \Lambda \mathbf{t}_{\text{coarse}}, \quad (10)$$

where \mathbf{U} is a unit matrix; Λ is a regularization coefficient and \mathbf{L} represents the matting Laplacian matrix [15]:

$$\mathbf{L}(i, j) = \sum_{x|(i, j) \in w_x} \left(\delta_{ij} - \frac{1}{|w_x|} \left(1 + (I_i - \mu_x)^T \left(\Sigma_x + \frac{\epsilon}{|w_x|} U \right)^{-1} (I_j - \mu_x) \right) \right). \quad (11)$$

Suppose the coordinates of a point x in the image is (i, j) ; I represents the original image; δ_{ij} is the Kronecker delta; Σ_x is color covariance the of area w_x ; μ_x is the mean color value of area w_x ; and ϵ is a regularization coefficient. Figure 5 shows the depth map after mosaic distortion was improved by image matting.

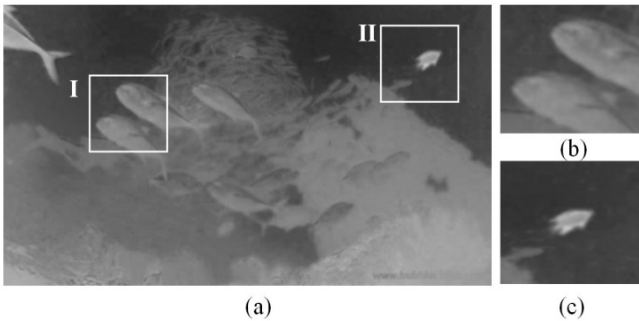


Fig. 5. (a) Depth Map after Improvement with Image Matting; (b) Blow Up of Frame I; (c) Blow Up of Frame II; in comparison with Fig. 4(b) and 4(c), the improved depth map captures the contours of image objects more accurately

After correcting the original image to obtain a more accurate $d(x)$, the distance between the object and the camera, Eq. (1) is employed to remove hazing effects and restore a portion of the color cast. The underwater image $J_\lambda(x)$ was:

$$J_\lambda(x) = \frac{I_\lambda(x) - B_\lambda}{t_\lambda(x)} + B_\lambda, \lambda \in \{R, G, B\}. \tag{12}$$

As can be seen in Fig. 6, subsequent to compensating the haze and color cast caused by the distance between the objects and the camera, a further estimation of the distance between the objects and the water surface D was required to calibrate the color cast caused by water depth.



Fig. 6. Underwater Image after Eliminating Haze and Some Color cast Caused by $d(x)$; a bluish offset still exists

2.2 Underwater Depth of the Photographic Scene D

Suppose the energy of each wavelength in light beam A from the air is $E_A(R)$, $E_A(G)$, and $E_A(B)$. After penetrating underwater depth D , the energy of each wavelength after attenuation becomes the background light B : $E_B(R)$, $E_B(G)$, and $E_B(B)$. To estimate underwater depth D , background light B is first detected. The image location in correspondence with background light B can be estimated with dark channel prior [14]. Depth D is the depth with the minimum error between the background light energy $E_B(R)$, $E_B(G)$, and $E_B(B)$ and incident light energy from the air $E_A(R)$, $E_A(G)$, and $E_A(B)$ after attenuation to depth K (Eq. (3)).

$$\min_k \left\{ \begin{aligned} & \left\| \left(E_B(R, D) - E_A(R, 0) \times (Rer(R))^k \right) \right\| + \left\| \left(E_B(G, D) - E_A(G, 0) \times (Rer(G))^k \right) \right\| \\ & + \left\| \left(E_B(B, D) - E_A(B, 0) \times (Rer(B))^k \right) \right\| \end{aligned} \right\}. \tag{13}$$

Once D is determined, the amount of attenuation in each wavelength can be used to compensate the energy differences and restore the color cast distortion from depth D :

$$E(\hat{J}_\lambda) = \frac{E(J_\lambda)}{Rer(\lambda)^D}, \lambda \in \{R, G, B\}, \tag{14}$$

where is the underwater image after haze removal and calibration of color cast, as shown \hat{J}_λ in Figure 7. However, the depth of the top and bottom of the image are not

the same; using depth D for energy compensation of the entire image results in some color cast remaining at the bottom of the image. Thus, depth estimation for each point in the image is necessary to achieve corresponding energy compensation at the various depths.



Fig. 7. Underwater Image after Removing Color cast and Color Scatter from Distance $d(x)$ and Depth D ; as the depths of the top and bottom of the image are different, color cast distortion still exists at the bottom of the image

2.3 Image Depth Range R

The depth range of the image covers the photographic scene from depth D to $D+R$, as shown in Figure 2. As light transmits through the depth range R , the different underwater depths induce differences in color cast at the top and bottom of the image, thereby necessitating varied energy compensation that corresponds to the underwater depth of each point to rectify color cast. During depth estimation in the depth range R , the foreground and background must first be separated to prevent the colors of the objects in the image from interfering with the estimation. The background of the image is natural light that travels directly to the camera without reflecting off objects; therefore using the background for estimation allows underwater depths to be calculated more accurately.

$$type(x) = \begin{cases} foreground & \text{if } d(x) > \sigma, \\ background & \text{if } d(x) \leq \sigma, \end{cases} \quad (15)$$

where σ is an adjustable coefficient and $d(x)$ is the distance between the object and the camera.

The background light B which is light that attenuated during passage to depth D is located at the very top of the image background. Taking a pixel at the bottom of the image background as d_{bottom} , the corresponding underwater depth is $D+R$. Background light B and point d_{bottom} are respectively located at the top and bottom of the depth range. The underwater depth of point x in the image is between D and $D+R$ and can be obtained by linear interpolation between background light B and point d_{bottom} . The corresponding underwater depth of point d_{bottom} is derived from Eq. (13).

Suppose x is situated on the x_j^{th} scan line; background light B is on the b^{th} scan line; and d_{bottom} is on the c^{th} scan line. The underwater depth of x in the actual scene $\delta(x_j)$ can be derived by linear interpolation between background light B and point d_{bottom} :

$$\delta(x_j) = D + \left(r \times \frac{(x_j - b)}{(c - b)} \right). \tag{16}$$

Once the underwater depth $\delta(x_j)$ of any given point x is obtained, the energy attenuation model is employed in energy compensation of the foreground and background in image $I_\lambda(x)$:

$$E(\hat{I}_\lambda(x)) = \frac{E(I_\lambda(x))}{\text{Re}r(\lambda)^{\delta(x_j)-D}}, \lambda \in \{R, G, B\}. \tag{17}$$

Figure 8 demonstrates the result of fine-tuning the amount of wavelength compensation by deriving the water depth of every image pixel. In comparison with Fig. 7, the color shift suffered at the lower part of the image is greatly reduced. Color balance is restored for the whole image, rather than just the top portion of the frame.



Fig. 8. Underwater Image after Eliminating Color cast from Image Depth Range

2.4 Artificial Light Source L

Artificial light sources are often supplemented to avoid insufficient lighting commonly encountered in underwater photographic environment, as shown in Fig. 9. If an artificial light source L is employed during image capturing process, the luminance contributed by L must be deducted first to avoid over-compensation for the stages followed, as illustrated in Fig. 10. The existence of artificial lighting can be determined by the difference between the mean luminance of the foreground and the background, L_f and L_b . In an underwater image without artificial lighting, the background directly transmits natural light without reflecting off of objects and is therefore the brighter part of the image. Higher mean luminance in the foreground of an image than in the background indicates the existence of an artificial light source. The difference between L_f and L_b is also the luminance of the artificial light source; that is to say, the luminance of the artificial light source is:

$$L(\lambda) = L_f(\lambda) - L_b(\lambda). \tag{18}$$

Supposing the artificial light radiates spherically, the influence of the light is in inverse proportion with the square of the distance. The closer the object, the more it is

affected by the artificial light source, and vice versa. After incorporating the variable of artificial light source, Eq. (17) can be rewritten as:

$$E(\hat{I}_\lambda(x)) = \frac{E(I_\lambda(x))}{\text{Rer}(\lambda)^{\delta(x_j)-D}} - (L(\lambda) \times (1 - d(x)^2)), \lambda \in \{R, G, B\}. \quad (19)$$

The result following removal of the effects of the artificial light source L is shown in Fig. 11.



Fig. 9. Illuminated by an artificial light source, the intensity of the foreground appears brighter than that of the background



Fig. 10. When the luminance contributed by an artificial light source is not deducted first, an over-exposed image will be obtained after the compensation stages followed



Fig. 11. The underwater image obtained after removing the artificial lighting present in Fig. 10

3 Experiment

Figure 12(a) was captured from a underwater video on the Youtube website filmed by the Bubble Vision Co. [16]. This AVI format video is 350 seconds long with a resolution of 720 p. Figure 12(b) shows the result after processing with a traditional dehazing algorithm [9]. Although the contrast of the image has increased, the color cast is more apparent as the attenuated energy was not individually compensated according to wavelength. Figure 12(c) shows the image after histogram equalization processing [12], from which haze effects and color cast still remain. Figure 12(d) shows the image after processing with the WCID method proposed in this study. The process effectively restored image color and removed haze effects, giving the image the original color and definition it would have had if it was not underwater. The *Rer* values used in the WCID in this study for red light, green light, and blue light were 82 %, 95 %, and 97.5 %.

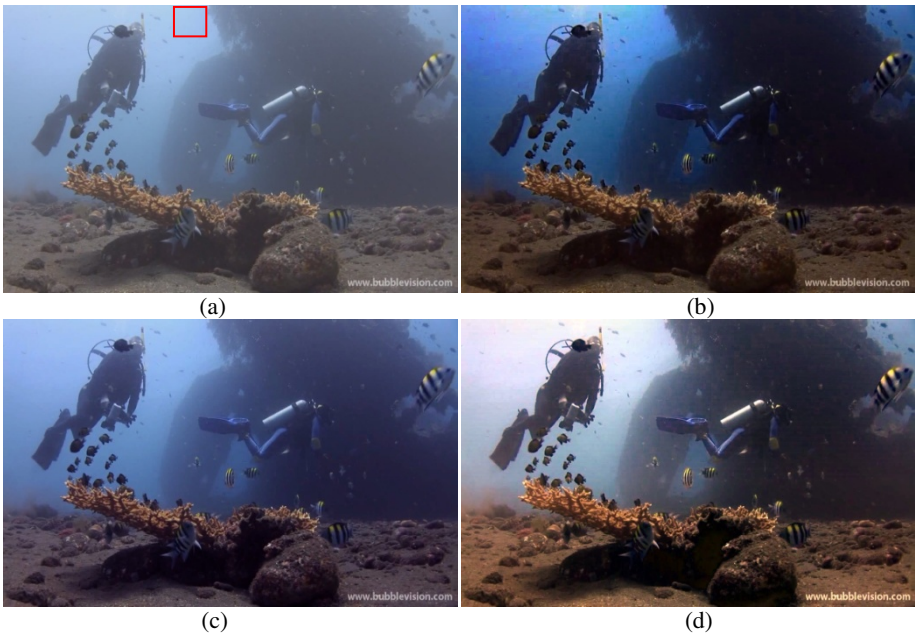


Fig. 12. (a) Original Input Image; the frame corresponds to the automatically estimated background light; (b) Image after Processing with Traditional Dehazing Algorithm; (c) Image after Processing with Histogram Equalization; (d) Image after Processing with WCID; the underwater depth of the scene in the image ranges approximately from 10 to 14 meters

4 Conclusion

The WCID algorithm proposed in this study can effectively restore image color and remove haze. However, the salt ratio and amount of suspended particles in ocean

water varies with time, location, and season, making accurate estimation of the rate of energy attenuation problematic. In addition, it is presumed that artificial light sources produce spherically radiating light different to surface light sources generally used in underwater photography; therefore the value of luminance is also difficult to estimate accurately. Future researchers may like to obtain a sample of ocean water and data on artificial light sources to further improve image restoration processes.

References

1. Junku, Y., Michael, W.: Underwater Robotics. *J. Advanced Robotics* 15(5), 609–639 (2001)
2. Ronald Zaneveld, J., Pegau, W.: Robust underwater visibility parameter. *J. Optics Express* 11, 2997–3009 (2003)
3. Van Rossum, M.C.W., Nieuwenhuizen, T.M.: Multiple scattering of classical waves: microscopy, mesoscopy and diffusion. *J. Rev. Mod. Phys.* 71(1), 313–371 (1999)
4. Houghton, J.T.: *The Physics of Atmospheres*. Cambridge University Press, London (2001)
5. McFarland, W.N.: Light in the sea—correlations with behaviors of fishes and invertebrates. *J. American Scientist Zoology* 26, 389–401 (1986)
6. Duntley, S.Q.: Light in the Sea. *J. Optical Society of America* 53(2), 214–233 (1963)
7. Jerlov, N.G.: *Optical Oceanography*. Elsevier Publishing Company, Amsterdam (1968)
8. Schechner, Y.Y., Karpel, N.: Clean Underwater Vision. In: *IEEE Conference on Computer Vision and Pattern Recognition*, vol. 1, pp. 536–543. IEEE Press, USA (2004)
9. Chao, L., Wang, M.: Removal of Water Scattering. In: *International Conference on Computer Engineering and Technology*, vol. 2, pp. 35–39. IEEE Press, India (2010)
10. Weilin, H., Gray, D.J., Weidemann, A.D., Fournier, G.R., Forand, J.L.: Automated underwater image restoration and retrieval of related optical properties. In: *International Geoscience and Remote Sensing Symposium*, vol. 1, pp. 1889–1892. IEEE Press, Spain (2007)
11. Yamashita, A., Fujii, M., Kaneko, T.: Color Registration of Underwater Image for Underwater Sensing with Consideration of Light Restoration. In: *International Conference on Robotics and Automation*, pp. 4570–4575. IEEE Press, Italy (2007)
12. Iqbal, K., Abdul Salam, R., Osman, A., Zawawi Talib, A.: Underwater image enhancement using an integrated color model. *J. Computer Science* 34, 2–12 (2007)
13. Fattal, R.: Single Image Dehazing. In: *International Conference on Computer Graphics and Interactive Technique*, vol. (72), pp. 1–9. ACM SIGGRAPH Press, USA (2008)
14. He, K., Sun, J., Tang, X.: Single image haze removal using Dark Channel Prior. In: *IEEE Conference on Computer Vision and Pattern Recognition*, vol. 1, pp. 1956–1963. IEEE Press, USA (2009)
15. Levin, A., Lischinski, D., Weiss, Y.: A closed form solution to natural image matting. In: *IEEE Conference on Computer Vision and Pattern Recognition*, vol. 1, pp. 61–68. IEEE Press, USA (2006)
16. Bubblevision Underwater Image,
<http://www.youtube.com/user/bubblevision>